A&A 531, A133 (2011)
DOI: 10.1051/0004-6361/201014213

Astronomy & Astrophysics

High-resolution spectroscopic observations of the metal-poor, chemically peculiar, and high velocity Fehrenbach & Duflot star⋆,⋆⋆

N. A. Drake[1] and C. B. Pereira[2]

[1] Sobolev Astronomical Institute, St. Petersburg State University, Universitetski pr. 28, St. Petersburg 198504, Russia
[2] Observatório Nacional, Rua José Cristino, 77, CEP 20921-400, São Cristóvão, Rio de Janeiro-RJ, Brazil
e-mail: [drake,claudio]@on.br

Received 6 February 2010 / Accepted 5 May 2011

ABSTRACT

Aims. We determine the atmospheric parameters and abundance pattern of the chemically peculiar metal-poor Fehrenbach & Duflot (Feh-Duf) star to more clearly understand its evolutionary state and the nature of the s-element enhancement in this star.
Methods. Its atmospheric parameters and chemical abundances were determined using high resolution optical spectroscopy and employing the local-thermodynamic-equilibrium model atmospheres of Kurucz and spectral analysis code MOOG.
Results. The derived abundances show that the Feh-Duf star is a low-metallicity ([Fe/H] = −1.93) star with high carbon and heavy s-element abundances, while the abundance of the light s-process element yttrium is low ([Y/Fe] = −0.07). The oxygen abundance is lower than for Galactic halo stars of similar metallicity.We conclude that the Feh-Duf star could be a CH star with C/O = 1.3. Another possibility is that the Feh-Duf star could be an early-AGB star. The Fehrenbach & Duflot star is also a lead star with [Pb/Ce] = +0.69. In addition, it displays an extreme retrograde motion ($V_{\rm GRF}$ = −259 km s^{-1}), which in combination with its underabundance of α-elements suggests that this star may have been captured by the Milky Way galaxy.

Key words. stars: abundances – stars: individual: Feh-Duf – stars: chemically peculiar – stars: population II – stars: kinematics and dynamics – stars: fundamental parameters

1. Introduction

The Fehrenbach & Duflot star (=2MASS J05025386-6544207, hereafter the Feh-Duf star according to SIMBAD designation) was discovered in 1981 by Fehrenbach & Duflot (1981) during their measurements of radial velocities of stars in the region of the Large Magellanic Cloud. They found that this star has a very high radial velocity (+440 km s^{-1}) and also displays exceedingly strong CH absorption bands in its spectrum. These spectral characteristics are typical of CH stars, a group of peculiar late-type population II giants whose overabundance of carbon and of s-process elements is explained by mass-transfer in a binary system from a former asymptotic giant branch (AGB) star that is now a white dwarf. In this work, we present a high-resolution spectroscopic study of the Feh-Duf star to determine its abundance pattern and discuss its evolutionary state as well as a possible extragalactic origin for this star.

2. Observations

The high-resolution spectra of the Feh-Duf star analysed in this work were obtained with the FEROS (Fiberfed Extended Range Optical Spectrograph) echelle spectrograph (Kaufer et al. 1999) at the 2.2 m ESO telescope at La Silla (Chile) on the night of October 20, 2008. The FEROS spectral resolving power is R = 48 000, corresponding to 2.2 pixels of 15 μm, and the wavelength coverage goes from 3800 Å to 9200 Å. The nominal signal-to-noise ratio (hereafter S/N) was evaluated by measuring the rms flux fluctuation in selected continuum windows, and the typical value being found to be S/N = 100−150 after two exposures of 3600 s. The spectra were reduced with the MIDAS pipeline reduction package consisting of the following standard steps: CCD bias correction, flat-fielding, spectrum extraction, wavelength calibration, correction of barycentrer velocity, and spectrum rectification. Figure 1 shows the spectrum of the Feh-Duf star in the 6130−6170 Å region. A strong redshift of about 9.2 Å is observed.

3. Analysis and results

3.1. Line selection, measurements, and oscillator strengths

The atomic absorption lines selected in this study are basically the same as those used in previous studies devoted to the analysis of the photospheric abundances of chemically peculiar stars (Pereira & Drake 2009). The selected lines are sufficiently unblended to yield reliable abundances. Table 1 shows the Fe I and Fe II lines employed in the analysis, the lower excitation potential χ of the transitions, the $\log gf$ values, the measured equivalent widths EW_λ and the derived iron abundances of each line. The latter were obtained by fitting Gaussian profiles to the observed ones. The $\log gf$ values for the Fe I and Fe II lines given in Table 1 were taken from Lambert et al. (1996).

⋆ Based on observations made with the 2.2 m telescope at the European Southern Observatory (La Silla, Chile).
⋆⋆ Tables 1 and 3 are available in electronic form at http://www.aanda.org

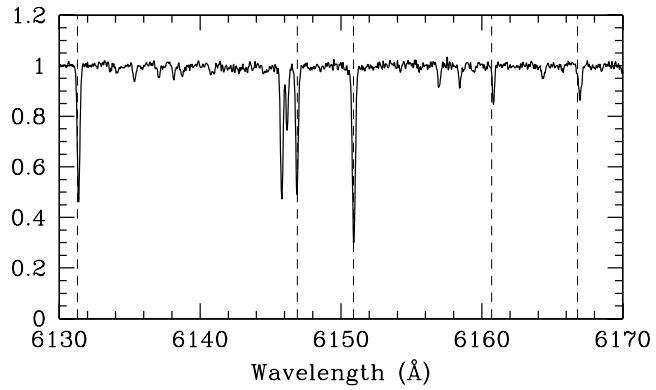

Fig. 1. Spectrum of the Feh-Duf star analyzed in this work. Short dashed vertical lines show the transitions of Ca I 6122.23, Fe I 6137.70, Ba II 6141.73, Fe I 6151.62, and Fe I 6157.73. The spectral lines are strongly shifted toward the red by about 9.2 Å because of the radial velocity of 448.3 km s^{-1}.

Table 2. Atmospheric parameters, radial velocity, and Galactic latitude of Feh-Duf.

Parameter	Value
$T_{\rm eff}$ (K)	4500 ± 120
log g (dex)	0.9 ± 0.2
[Fe/H] (dex)	−1.93 ± 0.10
ξ (km s^{-1})	1.9 ± 0.3
V_r (km s^{-1})	+448.3 ± 0.6
gal. latitude (b°)	−35.6

3.2. Determination of the atmospheric parameters

The determination of atmospheric parameters, effective temperature ($T_{\rm eff}$), surface gravity (log g), microturbulence (ξ), and metallicity ([Fe/H]) (throughout, we use the notation [X/H] = $\log(N({\rm X})/N({\rm H}))_\star - \log(N({\rm X})/N({\rm H}))_\odot$) are prerequisites for abundance determination. To derive these parameters, we followed exactly the procedures described in previous studies of chemically peculiar stars (Drake & Pereira 2008; Pereira & Drake 2009). The final derived atmospheric parameters of the Feh-Duf star are given in Table 2.

The internal errors in the adopted effective temperature ($T_{\rm eff}$) and microturbulent velocity (ξ) can be determined from the uncertainty in the slope of the Fe I abundance versus excitation potential and Fe I abundance versus reduced equivalent width (EW_λ/λ) relations. These quantities are given in Table 2. The standard deviation in log g was set by varying this parameter around the adopted solution until the Fe I and Fe II mean abundances differed by exactly one standard deviation of the [Fe I/H] mean value. The value of log g quoted in Table 2 was determined by means of ionization balance using the assumption of local thermodynamic equilibrium (hearafter LTE). On the other hand, it is well-known that for low-gravity and low-metallicity stars Fe I abundance is subject to significant non-LTE (hereafter NLTE) effects (e.g. Korn et al. 2003; Thevenin & Idiart 1999, and references therein). However, a consensus of the expected magnitude of NLTE effects has not yet been achieved and a full discussion of NLTE effects is beyond the scope of this paper. Mashonkina et al. (2011) carried out a detailed study of the NLTE mechanisms affecting the formation of neutral and singly-ionized iron lines in stellar atmospheres, covering a broad range of effective temperatures, gravities, and metallicities. These authors have developed a comprehensive atomic model for neutral and singly-ionized iron and found that NLTE leads to positive abundance corrections, in agreement with previous studies. However, the magnitude of the corrections that they found is smaller than had been found in earlier results. For example, for the very low metallicity cool giant HD 122563 ($T_{\rm eff}$ = 4600 K, log g = 1.60, [Fe/H] = −2.50), they found that the average NLTE abundance correction amounts to +0.10 dex for Fe II lines and +0.19 dex for Fe I lines. Assuming that LTE leads to a discrepancy in the abundances inferred for Fe II and Fe I of about 0.1 dex, we estimated its influence on the surface gravity determination to be +0.25. In Sect. 3.4, we estimate the effects of this uncertainty in log g on the derived abundances.

3.3. Abundance analysis

The abundances of chemical elements were determined with LTE model-atmosphere techniques. In brief, equivalent widths were calculated by integration through a model atmosphere and were then compared with the observed equivalent widths. This calculation is repeated, changing the abundance of the element in question, until a match is achieved. The LTE atmosphere models of Kurucz (1993) and the current version of the line-synthesis code MOOG (Sneden 1973) were used to carry out the calculations.

Table 3 shows the atomic lines used to derive the abundances of the elements as well as the abundances derived for each individual line and Table 4 provides the number of lines employed (or the number of spectral regions in the case of carbon and nitrogen whose abundances were determined using molecular lines) for each species, n, the derived abundances with their respective standard deviations, and the [X/H] and [X/Fe] ratios as well as the C/O and the carbon isotopic ^{12}C/^{13}C ratio.

The abundance of manganese is based on the Mn I lines λ5420 and λ6021 Å. All fine-structure and hyperfine-structure components for the lines of Mn I were explicitly included. The gf-values for the Mn I lines were taken from del Peloso et al. (2005).

The lead abundance was derived from the Pb I line at λ4057.81 Å. The line data, which include isotopic shifts and hyperfine splitting, were taken from Van Eck et al. (2003).

Carbon, nitrogen, and oxygen abundances, as well as the ^{12}C/^{13}C isotopic ratio, were also determined using the spectrum synthesis technique. Since the abundances of the CNO elements are interdependent because of the association of carbon and oxygen in CO molecules in the atmospheres of cool giants, the CNO abundance determination procedure was iterated until all the abundances of these three elements agreed. The abundances of carbon, nitrogen, and the ^{12}C/^{13}C isotopic ratio were determined using the lines of the CH, CN, and C_2 molecules. The line lists were assembled by ourselves are similar to those of Drake & Pereira (2008) and Pereira & Drake (2009) who studied the chemically peculiar metal-poor stars HD 104340, HD 206983, HD 10613, and BD+04°2466. Nevertheless, studying the Fehrenbach & Duflot star we have updated the value of the dissociation potential of the CN molecule. In the above mentioned papers, we used the value D_0(CN) = 7.65 eV determined by Engleman & Rouse (1975). More recent studies based on experimental determinations (Huang et al. 1992; Costes et al. 1990) as well as on theoretical calculations (Pradhan et al. 1994), showed that the dissociation energy of the CN molecule is higher, about 7.75 eV, and this value was used in the synthetic spectra calculations.

Table 4. Chemical abundances derived for the Feh-Duf star in the scale $\log \varepsilon(\mathrm{H}) = 12.0$ and in the notations [X/H] and [X/Fe].

Species	n	$\log \varepsilon$	[X/H]	[X/Fe]
Fe I	47	5.59 ± 0.09	–1.93	—
Fe II	9	5.58 ± 0.08	–1.94	—
C (C_2)	syn	7.21 ± 0.05	–1.31	+0.62
N (CN)	syn	6.59 ± 0.20	–1.33	+0.60
O I	1	7.10 ± 0.03	–1.73	+0.20
Mg I	2	6.08	–1.50	+0.43
Si I	2	6.01	–1.54	+0.39
Ca I	11	4.72 ± 0.10	–1.64	+0.29
Sc II	6	1.31 ± 0.27	–1.86	+0.07
Ti I	6	3.07 ± 0.15	–1.95	–0.02
Cr I	5	3.63 ± 0.19	–2.04	–0.11
Mn I	2	2.99	–2.40	–0.47
Ni I	5	4.26 ± 0.18	–1.99	–0.06
Zn I	2	2.79	–1.81	+0.12
Y II	4	0.24 ± 0.12	–2.00	–0.07
Ba II	2	1.15	–0.98	+0.95
La II	3	0.00 ± 0.13	–1.17	+0.76
Ce II	7	0.54 ± 0.12	–1.04	+0.89
Nd II	14	0.50 ± 0.13	–1.00	+0.92
Pb I	1	1.61	–0.34	+1.58

Notes. C/O =1.26 ± 0.15. $^{12}C/^{13}C = 8.0 \pm 2.0$. The adopted solar abundances are from Grevesse & Sauval (1998).

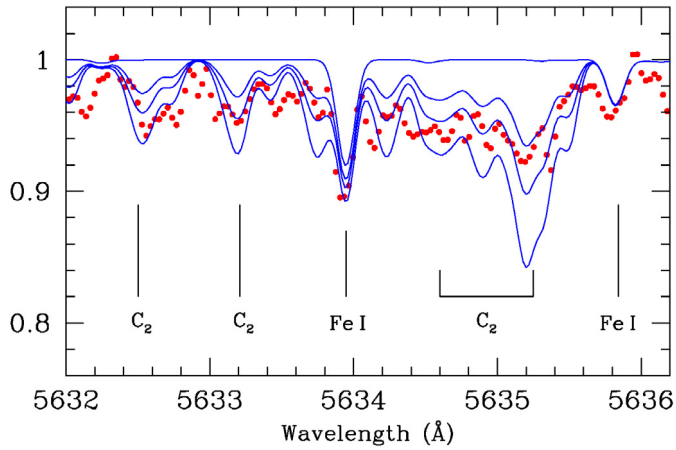

Fig. 2. Observed (dotted red line) and synthetic (solid blue line) spectra in the region around the C_2 molecule lines at 5635 Å. We show the synthesis for the carbon abundances $\log \varepsilon(\mathrm{C}) = 7.16$, 7.21, and 7.26. The upper line corresponds to the spectrum calculated without any contribution from the C_2 lines.

Figure 2 shows the observed and synthetic spectra in the region around the C_2 (0, 1) band head of the Swan system $A^3\Pi_g - X^3\Pi_u$ at λ5635 Å. The oxygen abundance was inferred from the [O I] forbidden line at λ6300.304 Å. In our calculations for this line we used the oscillator strength $\log gf = -9.717$ obtained by Allende Prieto et al. (2001) in their analysis of the solar oxygen abundance.

Lithium abundance was derived from the synthetic spectra matches to the Li I λ6708 Å resonance doublet. Special attention was given to the identification of s-process element lines in the vicinity of the lithium line. Using the databases VALD (Kupka et al. 1999, and references therein) and D.R.E.A.M. (Database on Rare-Earths At Mons University, Biémont et al. 1999) we created a line list that is as complete as possible. For the lines appearing in both databases, the VALD oscillator strength values for the s-process element lines were replaced by those from the D.R.E.A.M. database. The CN lines in the vicinity of the Li I doublet were included in the line list. The wavelengths and oscillator strengths for the individual hyperfine and isotopic components of the lithium lines were taken from Smith et al. (1998) and Hobbs et al. (1999). A solar $^6Li/^7Li$ isotopic ratio ($^6Li/^7Li = 0.081$) was adopted in calculations of the synthetic spectrum.

Table 5. Abundance uncertainties of the Feh-Duf star.

Species	$\Delta T_{\rm eff}$ +120 K	$\Delta \log g$ +0.2	$\Delta\xi$ +0.3	Δ [Fe/H] +0.1	ΔW_λ +3 mÅ	$\left(\sum \sigma^2\right)^{1/2}$	$\sigma_{\rm obs}$
Fe I	+0.20	–0.03	–0.10	+0.04	+0.06	0.23	0.09
Fe II	–0.03	+0.07	–0.04	–0.01	+0.06	0.10	0.08
Mg I	+0.23	–0.06	–0.17	+0.04	+0.05	0.30	—
Si I	+0.12	–0.03	–0.10	+0.03	+0.07	0.18	—
Ca I	+0.17	–0.03	–0.08	+0.03	+0.05	0.20	0.10
Sc II	+0.04	+0.07	–0.06	–0.02	+0.05	0.11	0.27
Ti I	+0.24	–0.03	–0.09	+0.04	+0.05	0.27	0.15
Cr I	+0.25	–0.03	–0.08	+0.03	+0.05	0.27	0.19
Mn I	+0.18	–0.03	–0.06	+0.02	+0.03	0.20	—
Ni I	+0.18	–0.02	–0.04	+0.02	+0.06	0.20	0.09
Zn I	+0.02	+0.02	–0.06	0.00	+0.06	0.09	—
Y II	+0.06	+0.05	–0.10	–0.02	+0.05	0.14	0.12
Ba II	+0.12	+0.05	–0.27	–0.02	+0.04	0.30	—
La II	+0.08	+0.07	–0.03	–0.04	+0.06	0.13	0.13
Ce II	+0.07	+0.05	–0.12	–0.01	+0.05	0.16	0.12
Nd II	+0.07	+0.06	–0.05	–0.02	+0.03	0.11	0.13

Notes. The second column gives the variation in the abundance caused by the variation in $T_{\rm eff}$. The other columns refer, respectively, to the variations due to $\log g$, ξ, [Fe/H] and W_λ. The seventh column gives the compounded rms uncertainty of the second to sixth columns. The last column gives the observed abundance dispersion for those elements whose abundances were derived using more than three lines.

3.4. Abundance uncertainties

Table 5 shows that neutral elements are rather sensitive to temperature variations. The singly ionized elements are also sensitive to variations in $\log g$. In the case of elements, such as barium, whose abundance is based on stronger lines, the error introduced by the microturbulence is significant. For the elements analyzed via spectrum synthesis, the same technique was used, by varying $T_{\rm eff}$, $\log g$, ξ, and [Fe/H] and computing the abundance changes introduced by the variation in these atmospheric parameters. The resulting uncertainties are also included in Table 5.

The abundance uncertainties arising from errors in the equivalent widths measurements were computed using expressions provided by Cayrel (1988). The errors in the equivalent widths are set, essentially, by the S/N and the spectral resolution. In our case, with $R \approx 48\,000$ and a typical S/N of 150, the expected uncertainties in the equivalent widths are about 2–3 mÅ. These error estimates were applied to the measured EW_λ's and the corresponding changes in the element abundances are listed in Col. 6 of Table 5.

We also estimated the influence of model errors, such as the uncertainties in the effective temperatures and surface gravities, on the derived CNO abundances. Moreover, as mentioned above, the abundances of the CNO elements are interdependent, the uncertainties in the oxygen abundance determination affecting the carbon abundance and vice versa. Uncertainties in the carbon

Table 6. Effect of errors in atmospheric parameters and carbon and oxygen abundances on the CNO abundances.

Species	$\Delta T_{\rm eff}$ +120 K	$\Delta\log g$ +0.2	$\Delta\xi$ +0.3	$\Delta\log$ (C) +0.1	$\Delta\log$ (O) +0.1	$\sigma_{\rm tot}$
C	+0.20	+0.01	0.00	–	+0.03	0.20
N	+0.33	0.00	0.00	−0.12	+0.05	0.35
O	0.00	+0.03	+0.01	0.02	–	0.04

Notes. The second to fourth columns give the variation in the abundances due to variations in $T_{\rm eff}$, $\log g$, and ξ. The fifth and sixth columns shows variations caused by variations in the C and/or O abundances.

abundance cause variations in the nitrogen abundance, because the CN molecule lines were used for the nitrogen abundance determination. The variations in the abundance caused by changes in the effective temperature (±120 K), surface gravity (±0.2 dex), and both C and O abundances (±0.1 dex) are summarized in Table 6. In the last column of this table, we present the resulting abundance uncertainties, $\sigma_{\rm tot}$, calculated as the square root of the sum of squares of the various sources of uncertainties. Derived CNO abundances are weakly sensitive to variations in the microturbulent velocity because weak lines were used for their determination. A further source of uncertainty in the molecular line analysis is the uncertainty in the molecule constants, in particular the dissociation energy of the CN molecule. Our tests showed that variations in the CN molecule dissociation energy of ΔD_0(CN) = +0.10 eV resulted in variations in the nitrogen abundance of about −0.1 dex. Calculations of the carbon isotopic ratios do not depend on the uncertainties in the C and N abundances and molecular parameters. The error in the ^{12}C/^{13}C determination comes mainly from uncertainties in the observed spectrum, such as possible contamination by unidentified atomic or molecular lines, or uncertainties in the continuum placement.

4. Discussion

4.1. Luminosity and distance of the Feh-Duf star

Since the parallax of the Feh-Duf star had not been measured, we estimated its luminosity and distance using theoretical evolutionary tracks. Assuming a stellar mass of 0.8 $M_\odot$ and using the evolution tracks of Fagotto et al. (1994), we obtained $\log L/L_\odot$ = 3.01 ± 0.20 or $M_{\rm bol}$ = −2.8 ± 0.5. Taking into consideration the observed magnitude of V = 11.78 and BC = −0.495 (Allonso et al. 1999) we obtained M_V = −2.3 ± 0.5 and $r = 5.9^{+1.5}_{-1.2}$ kpc. The reddening E_{B-V} = 0.06 determined for the LMC stars (Grieve & Madore 1986; Pompéia et al. 2008) was adopted. This value of the colour excess agrees well with the intensity of the interstellar Na I D_1 and D_2 lines of 126.9 mÅ and 176.1 mÅ, respectively, in the spectrum of the Feh-Duf star. Figure 3 displays the evolutionary tracks for several stellar masses in the $\log g - \log T_{\rm eff}$ plane at a metallicity of Z = 0.0004 computed by Fagotto et al. (1994). The position of the Feh-Duf star in this plane is also shown.

According to Table IV of Hartwick & Cowley (1985), CH stars have M_V values between −0.25 and −2.2, therefore the Feh-Duf star, with M_V = −2.3, could be a CH star and hence a binary star. It indeed displays characteristics of halo population: low metallicity, high radial velocity, and high galactic latitude. However, from the luminosity derived above, we cannot totally rule out the possibility that the Feh-Duf star could be an early-AGB star. Theoretical calculations show that for a star to be at this phase, it should have a luminosity of $\log L/L_\odot$ = 3.1 ($M_{\rm bol}$ = −3.1, Vassiliadis & Wood 1993).

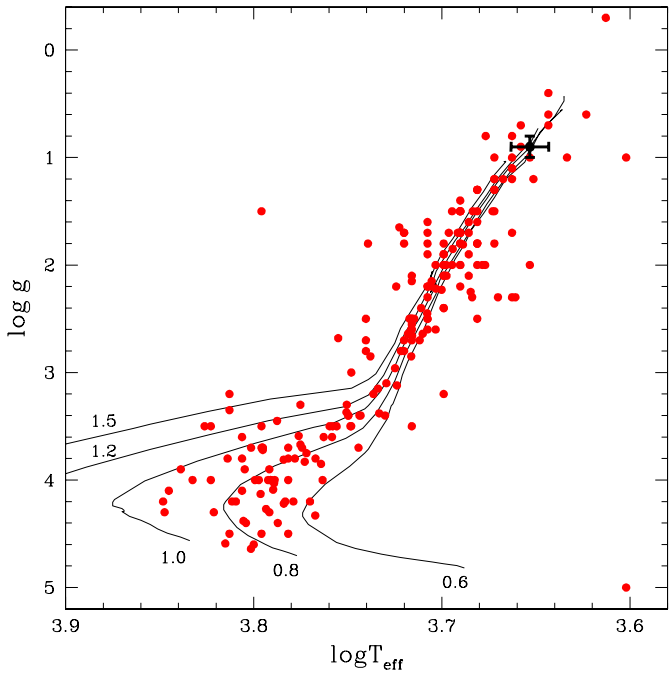

Fig. 3. Location of the Feh-Duf star in the ($\log T_{\rm eff}$, $\log g$) plane (filled circle with attached error bars). Evolutionary tracks (Fagotto et al. 1994) at metallicity Z = 0.0004 for stellar masses 0.6, 0.8, 1.0, 1.2, and 1.5 $M_\odot$ are plotted. Red circles represent the position of CEMP, CH and barium stars (Masseron et al. 2010).

We determined the radial velocity of the Feh-Duf star to be $v_{\rm rad}$ = +448.3 ± 0.6 km s^{-1}. This value is in good agreement with the value $v_{\rm rad}$ = +440 km s^{-1} obtained by Fehrenbach & Duflot (1981).

4.2. Kinematics

Assuming a distance of r = 5.9 kpc, we calculated the space-velocity components (U_0, V_0, W_0) for the Feh-Duf star using the algorithm of Johnson & Soderblom (1987). Proper motions were taken from NOMAD catalog (Zacharias et al. 2004). The obtained heliocentric space velocities are (U_0, V_0, W_0) = (−116, −491, −106) km s^{-1}. We transformed the V_0 component of the space velocity of the Feh-Duf star to the Galactocentric reference frame (GRF) using $(U, V, W)_\odot$ = (9, 232, 7) (Venn et al. 2004), which corresponds to $V_{\rm GRF}$ = −259 km s^{-1}. In Table 7, we present the space velocity components of the Feh-Duf star calculated for different (from 0.6 to 1.5 $M_\odot$) values of the stellar mass. The luminosities, and hence the distances, corresponding to the adopted masses were estimated from the above mentioned evolutionary tracks. The values of $V_{\rm GRF}$ shows that the Feh-Duf star has extreme retrograde motion. As pointed out by Marsakov & Borkova (2006), a star born in a monotonically collapsing single protogalactic cloud could not be in a retrograde orbit. This extreme retrograde motion of the Feh-Duf star may be a sign that this star was accreted by the Milky Way from a dwarf satellite galaxy.

Table 7. Space velocity components of the Feh-Duf star relative to the Sun (U_0, V_0, and W_0) and in the Galactic reference frame (V_{GRF}) calculated for different distances.

$M/M_\odot$	M_V	$\log L/L_\odot$	Dist kpc	U_0 km s^{-1}	V_0 km s^{-1}	W_0 km s^{-1}	V_{GRF} km s^{-1}
0.6	−2.0	2.88	5.1	−95.0	−473.2	−127.0	−241.2
0.8	−2.3	3.01	5.9	−116.3	−490.8	−105.8	−258.8
1.0	−2.5	3.10	6.6	−134.6	−505.9	−87.6	−273.9
1.5	−3.0	3.28	8.1	−172.6	−537.4	−49.7	−305.4

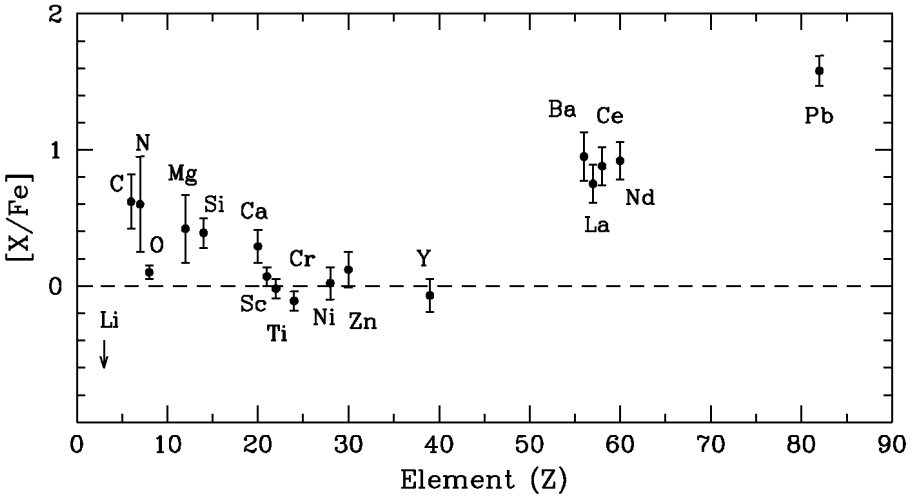

Fig. 4. Abundance pattern of the Feh-Duf star. Errors bars represent the uncertainty estimates described in the text.

4.3. Abundances

Below we discuss the abundance pattern of the Feh-Duf star by comparing it with previous studies for some halo population stars and also with the abundance patterns of chemically peculiar stars with heavy-element overabundances already reported in the literature. In addition, we also compare the abundance pattern of the Feh-Duf star with stars exhibiting retrograde motion already analyzed in the literature, as well as with stars belonging to dSph galaxies. Figure 4 shows the abundance pattern of the Feh-Duf star analyzed in this work.

4.3.1. Nitrogen and oxygen

Abundance surveys of dwarf stars show that there is no trend for the [N/Fe] versus [Fe/H] ratio, that is, in the metallicity range −2.0 < [Fe/H] < +0.3, [N/Fe] is ≈0.0 (Clegg et al. 1981; Tomkin & Lambert 1984; Carbon et al. 1987). As a star becomes a giant, nuclear processed material, due to the deepening of its convective envelope, is brought from the interior to the outer layers of the star changing the surface composition. As a consequence of the first dredge-up process, the abundance of ^{12}C is reduced and the abundance of nitrogen is enhanced (Lambert 1981). The nitrogen-to-iron ratio in the Feh-Duf star is high, [N/Fe] = 0.60 ± 0.20, although this value is less than the mean [N/Fe] ratio observed in the CH stars analyzed by Vanture (1992b), [N/Fe] = 1.3 ± 0.6.

Comparison of the oxygen-to-iron ratio in the Feh-Duf star with Galactic halo stars indicates that the [O/Fe] ratio in the Feh-Duf star is about 0.3 dex below the corresponding value for the stars of the same metallicity in the Galaxy (Nissen et al. 2002) (see Fig. 5).

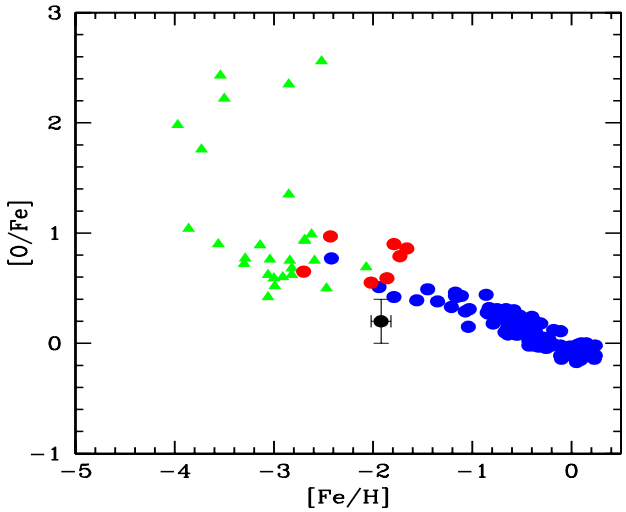

Fig. 5. [O/Fe] versus [Fe/H] for the Feh-Duf star (black circle), disk stars (blue circles), CEMP-s stars (red circles), and CEMP-no stars (green triangles). Abundance data for disk stars are from Edvardsson et al. (1993) and Nissen et al. (2002). Abundance data for CEMP-no stars are from Cayrel et al. (2004) and from Masseron et al. (2010) and abundance data for CEMP-s stars are from Masseron et al. (2010).

4.3.2. ^{12}C/^{13}C ratio

In Fig. 6, we show ^{12}C/^{16}O versus ^{12}C/^{13}C. In this figure, barium stars (red open squares) occupy a region between the GK-giants and C stars. They closely follow the sequence of GK giants passing through the S and SC types to become a carbon star along the TP-AGB phase. In CH subgiants, the ^{12}C/^{13}C ratio was investigated by Sneden (1983) and Drake & Pereira (2007). These two studies show that the ^{12}C/^{13}C ratio lies between 20 and 50. Compared to giants, this is taken as evidence that the first dredge-up has not yet started in these stars.

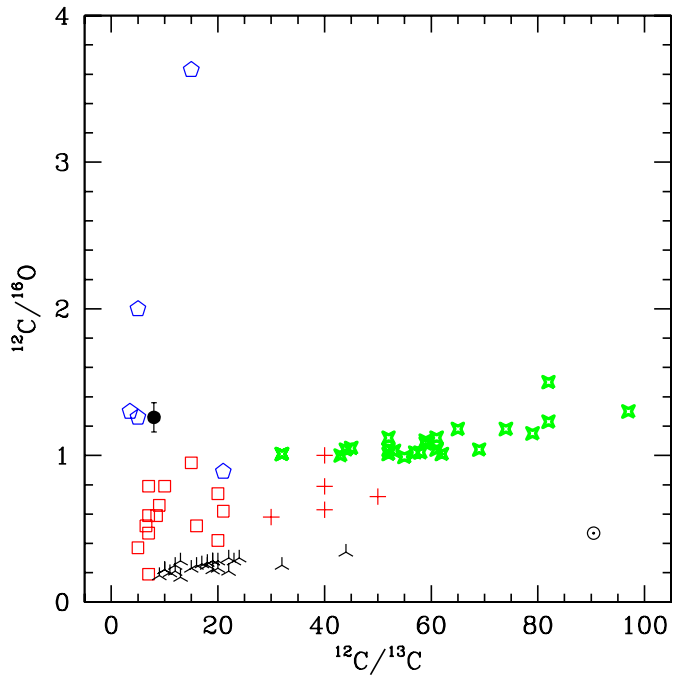

Fig. 6. $^{12}C/^{16}O$ versus $^{12}C/^{13}C$ ratios for several classes of stars and for the Feh-Duf star. Barium giants (red open squares); disk carbon stars, (green starry points); GK giants, (upside-down "Y"); CH stars, (blue open polygons); subgiant CH stars, (red plus sign) and Feh-Duf star (filled black circle).

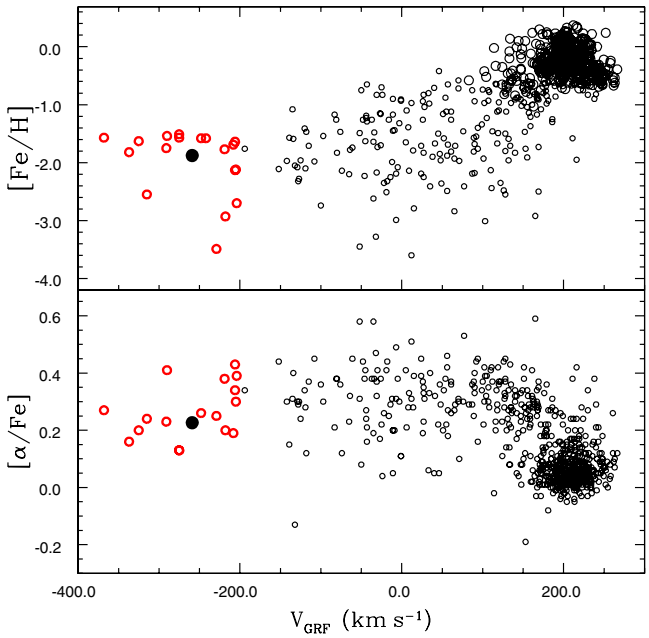

Fig. 7. Metallicity (*top*) and [α/Fe] (*bottom*) versus the V component of the space velocity relative to the Galactocentric Reference Frame for stars in the thin and thick discs, in the halo (black open circles) and those that exhibit extreme retrograde motion (red open circles). Filled black circle represents the Feh-Duf star.

The $^{12}C/^{13}C$ ratio in CH stars was investigated by Vanture (1992a), who showed that these stars could be divided into two groups according to the value of the $^{12}C/^{13}C$ ratio, some having $^{12}C/^{13}C \approx 3.0$ and others $^{12}C/^{13}C \geq 25.0$. For barium giants, the $^{12}C/^{13}C$ ratio lies between 8 and 20 (Barbuy et al. 1992; Drake & Pereira 2008; Pereira & Drake 2009). It remains to be verified, when the masses of CH stars and barium stars become available, whether this division in the $^{12}C/^{13}C$ ratios is related to mass. The star analyzed in this work, with $^{12}C/^{13}C = 8.0$, adds only one data point in this diagram but provides evidence that the Feh-Duf star is a CH star.

4.3.3. Iron group

Nickel abundance is expected to follow iron and does indeed with [Ni/Fe] = −0.02. The [Ni/Fe] ratio remains close to 0.0 in a metallicity range from −2.0 to 0.0 (Jonsell et al. 2005). The [Sc/Fe] ratio also does not exhibit any trend in the metallicity range $-3.0 \leq$ [Fe/H] ≤ 0.0 (Carretta et al. 2002) and the Feh-Duf star confirms this conclusion. The chromium-to-iron ratio also displays no trend for metal-poor stars. For the Feh-Duf star, the [Cr/Fe] ratio for the Feh-Duf star has a value typical for a metal-poor star with metallicity [Fe/H]≈ −2.0. The Mn deficiency is another indication that the Feh-Duf star belongs to a metal-poor population (Gratton 1989; Carretta et al. 2002). The Mn deficiency observed in the atmosphere of the Feh-Duf star is typical of halo field and globular clusters stars (Sobeck et al. 2006). Zinc was analyzed by Sneden et al. (1991) for disk and halo stars. Zinc abundance also follows the trend seen in the metallicity range between −2.5 and −0.5.

4.3.4. α-elements

The Feh-Duf star presents α-element abundance ([Mg+Ca+Ti/3Fe] = 0.23) lower than halo stars of the same metallicity (Carretta et al. 2002). Venn et al. (2004) analysed the chemical abundances of the stars in both the Galaxy and dwarf spheroidal (dSph) satellite galaxies. They confirmed that the [α/Fe] ratios in most stars of dSph galaxies are lower than in Galactic stars of similar metallicity. Figure 2 of Venn et al. (2004) shows that dSph stars are clearly separated from the majority of Galactic disk and halo stars. They also found that dSph's stars overlap with those stars of the Galactic halo that are in extreme retrograde orbits ($V_{GRF} < -200$ km s^{-1}). In Fig. 7, we reproduce Fig. 1 of Venn et al. (2004), where we see the position of the Feh-Duf star in the planes metallicity ([Fe/H]) versus V_{GRF} and [α/Fe] versus V_{GRF}. These diagrams and the low oxygen abundance seen in the Feh-Duf star support the hypothesis that this star may have been accreted by the Milky Way from a dwarf satellite galaxy.

4.3.5. Carbon and s-process elements

Figure 8 shows the [C/Fe] abundance ratio plotted as a function of the metallicity [Fe/H] for barium stars (giants and dwarfs), for CH stars, and for CEMP stars. We note that the Feh-Duf star has a lower [C/Fe] ratio as "expected" for a chemically peculiar binary star seen in this figure.

Figure 9 shows the [s/Fe] abundance ratio plotted as a function of the metallicity given by [Fe/H] for the same objects as in Fig. 8, for yellow symbiotic stars, and for the Feh-Duf star. Here "s" represents the mean of the elements created by slow neutron capture reactions (s-process): Y, Ba, La, Ce, Nd, and Pb. Among CEMP stars, there are six that are binaries i.e. CS 22942-019, CS 22948-027, CS 29497-030, CS 29497-034, CS 22964-161, and HE 0024-2523, The data for these stars concerning their heavy-element ($Z > 56$) overabundances and binarity have

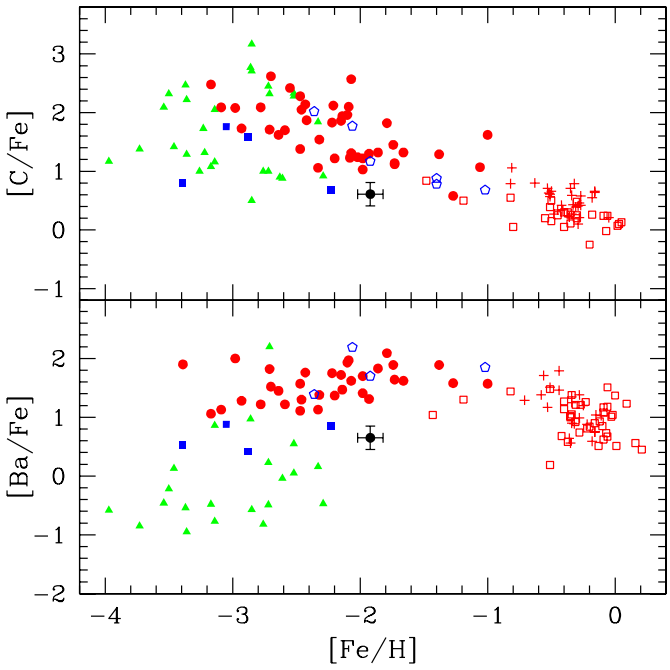

Fig. 8. Diagram of [C/Fe] versus [Fe/H] for several classes of chemically peculiar binary stars. Barium giants (red open squares); CH stars (blue open polygons); subgiant CH stars (red plus sign); and the Feh-Duf star (filled black circle). We also show the CEMP-s stars (red filled circles), the CEMP-no stars (green triangles) and the CEMP-low-s stars (Masseron et al. 2010) (blue filled squares).

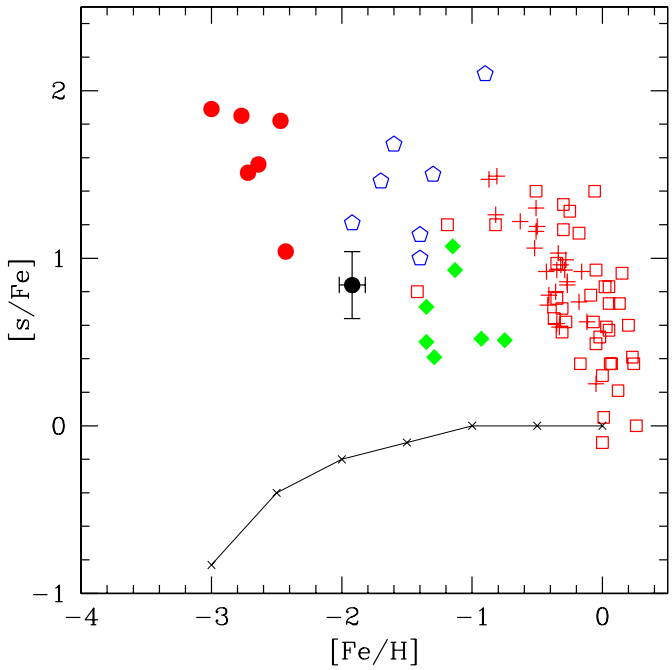

Fig. 9. Diagram of [s/Fe] versus [Fe/H]. The solid line is the *mean* ⟨[s/Fe]⟩ for field stars (Gratton & Sneden 1994; Ryan et al. 1996; and François et al. 2003). Green filled diamonds correspond to yellow-symbiotics, other symbols have the same meaning as in Fig. 8. For the CEMP-s stars, we show only those that have already been proven to be binary systems.

been taken from the recent results by Preston & Sneden (2001), Sivarani et al. (2004), Barbuy et al. (2005), Lucatello et al. (2003), Thompson et al. (2008), Aoki et al. (2002), and Hill et al. (2000). As we can see from this figure, the Feh-Duf star is enhanced in the s-process elements relative to metal-poor field stars. In the Feh-Duf star, the [element/Fe] ratio for each of these elements, except yttrium, is much higher than the same [element/Fe] ratios measured for metal-poor dwarfs, subgiant, and giant stars analysed by Gratton & Sneden (1994). The mean values of [Ba/Fe], [La/Fe], [Ce/Fe], and [Nd/Fe] at the metallicity of the Feh-Duf star is 0.0, while the same values for this star are +0.95, +0.76, +0.89, and +0.92, respectively. However, the abundance of light s-process elements, such as Y, is too low for a chemically peculiar binary system, such as CH stars and barium stars. In Table 2 of Busso et al. (2001), the ratio [ls/Fe] ("light s-elements") given by the mean abundance of Y and Zr, lies in the range between +0.2 and +1.3. In the Feh-Duf star, this ratio is given only by the [Y/Fe] ratio ([Y/Fe] = −0.02). According to Clayton (1988), Busso et al. (1999), Travaglio et al. (2004), and Venn et al. (2004), the neutron-capture nucleosynthesis in AGB stars is metallicity dependent. The first-peak elements (such as Y and Zr) are bypassed in favor of the second-peak elements and those from the third peak. The observed high [Ba/Y] ratio is consistent with the expectations for metal-poor AGB s-process yields. For the [Pb/Ce] ratio the proton-mixing scenario confirms the trend seen in several CH stars with high lead abundances (Van Eck et al. 2003; Goriely & Mowlavi 2000), although there is still a scatter in the [Pb/Ba] ratio for low-metallicity stars down to [Fe/H] = −2.5 (Masseron et al. 2010).

The lead abundance was determined using a spectral synthesis technique. Figure 10 shows the observed and synthetic spectra of the Feh-Duf star around Pb I λ4058 Å. In Fig. 11, we show the [Pb/Ce] ratio as a function of metallicity ([Fe/H]).

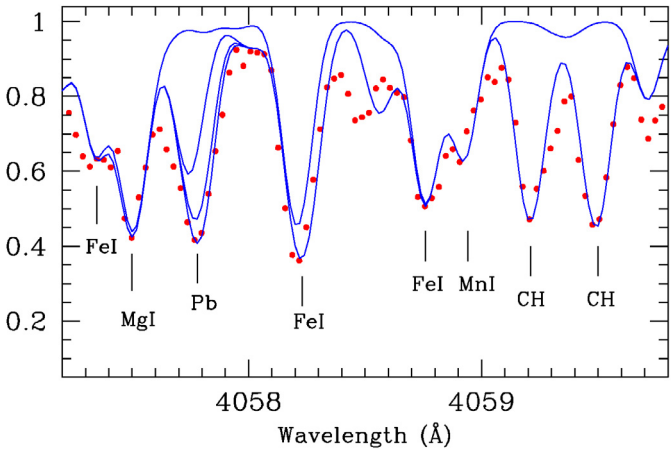

Fig. 10. Observed (dots) and synthetic (lines) spectra of Feh-Duf in the region around the Pb I line at λ4057.8 Å. The synthetic spectra are shown for lead abundances of log ε(Pb) = 0.10, 1.40, and 1.75. The upper line shows a synthesis without contribution from the CH molecule lines.

In this figure, we show the Feh-Duf star (the filled black circle at [Fe/H] = −1.93), the CH stars analyzed by Van Eck et al. (2003), CEMP stars that are members of binary systems, and the barium giants and dwarfs from Allen & Barbuy (2006). The solid line represents the prediction from the standard partial mixing (PM) model as given by Goriely & Mowlavi (2000). The position of the Feh-Duf in this diagram, follows the same trend as the other barium dwarfs and giants investigated so far.

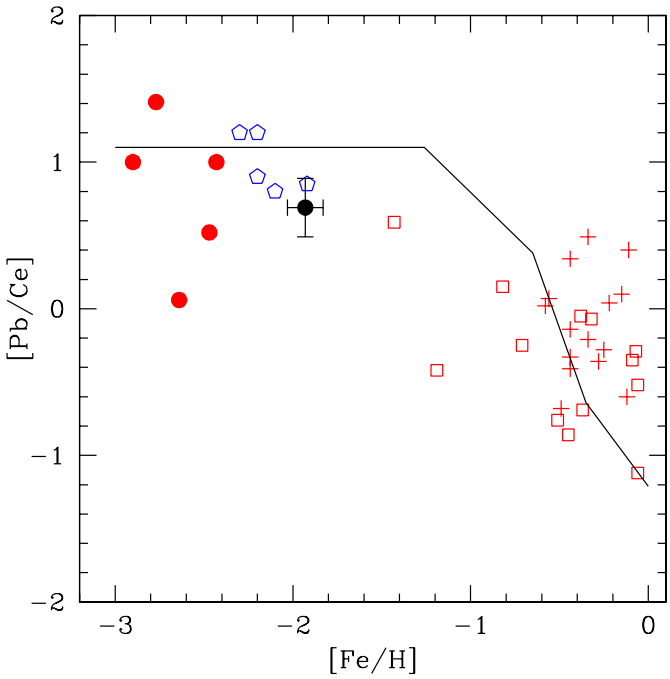

Fig. 11. The behaviour of the [Pb/Ce] ratio with metallicity. Symbols have the same meaning as in Fig. 8. The solid line represents the prediction from the standard partial mixing (PM) model as given by Goriely & Mowlavi (2000). For CEMP-s stars, we considered only those that have already been proven to be binary systems.

5. The Feh-Duf star compared with CH and CEMP stars

As shown above, the Feh-Duf is a low-metallicity star with high carbon and s-element abundances. Therefore, it is interesting to compare it with the CH and some CEMP stars already investigated in the literature. Unfortunately, we were unable to detect any Eu lines suitable for abundance determination of this element, which is mainly produced by the r-process, and permits us to separate different subclasses of CEMP stars according to the [Ba/Eu] ratio (Beers & Christlieb 2005; Masseron et al. 2010).

Besides to be an extragalactic candidate due to its observed kinematics and low [O/Fe] and [α/Fe] ratios relative to metal-poor stars in the Galaxy, the abundance pattern of the Feh-Duf star presents another peculiarity, namely, a lower barium and carbon abundance compared to CEMP stars at this metallicity. Figure 8 shows the [C/Fe] and [Ba/Fe] ratios plotted as a function of metallicity for CEMP stars (CEMP-no, CEMP-s, and CEMP-low-s) from Masseron et al. (2010). In both diagrams of Fig. 8, the Feh-Duf star is slightly below the CEMP stars. From its position in the $\log g - \log T_{\rm eff}$ plane, we see that the Feh-Duf star is one of the most evolved objects compared to stars in the sample of CEMP stars. In a way similar to CS 30322-023, which is another evolved object (Masseron et al. 2006), its carbon and barium enhancement is only moderate, permiting us to classify Feh-Duf as a CEMP-low-s star. As shown by Shetrone et al. (2010), the [C/Fe] ratio shows a plateau at low luminosity, followed by a decline in stars brighter than the "bump" of the RGB luminosity function caused by extra mixing acting after the bump. This extra mixing (regardless of its physical mechanism) may be responsible for the decrease in carbon and s-element abundances in the photospheres of the most evolved CEMP stars.

6. Conclusions

The abundance analysis performed by employing high-resolution optical spectra of the Feh-Duf star helped us to obtain its abundance pattern and carbon isotopic ratio. Our main conclusions can be summarized as follows:

1. The extreme retrograde motion ($V_{\rm GRF} = -259$ km s^{-1}) and chemical abundances of the α- and light-s elements distinct from those of Galactic halo stars of the same metallicity may suggest that the Feh-Duf star has an extragalactic origin and was captured by the Milky Way. It is interesting to notice that the Feh-Duf star displays similar trends for its s-process element abundances as the extragalactic carbon star, ALW-C7, analyzed by Abia et al. (2008): i.e. a lower Y and Zr abundances compared to heavy s-elements.
2. We have assumed that the Feh-Duf star has a mass of 0.8 $M_{\odot}$ to be compatible with the low metallicity, [Fe/H] = −1.93, determined for this star. The Feh-Duf star can either be a CH star (with C/O = 1.26) or a star at the early AGB phase since its luminosity is compatible with a star at this phase. In addition, as shown by Masseron et al. (2006), it is not improbable to find an AGB star in the halo. The luminosity of the Feh-Duf star is at the low limit of luminosities of AGB stars, with luminosities exceeding $\log(L/L_{\odot}) \sim 3$–4 (Ryan et al. 2005). The Feh-Duf star has no detected radial velocity variation (although this conclusion is based on only two measurements). However, as shown by Lucatello et al. (2005) who analysed the observed radial velocity data for a sample of 19 CEMP-*s* stars, an observed binary fraction of 68% is consistent with all CEMP-*s* stars being in multiple systems.
3. The Feh-Duf star is also a "lead star" since its lead-to-cerium ratio is high ([Pb/Ce] = +0.70) and closely follows the theoretical predictions for a star of this metallicity.

References

Abia, C., de Laverny, P., & Wahlin, R. 2008, A&A, 481, 161
Allen, D. M., & Barbuy, B. 2006, A&A, 454, 895
Allende Prieto, C., Lambert, D. L., & Asplund, M. 2001, ApJ, 556, L63
Allonso, A., Arribas, S., & Martínez-Roger, C. 1999, A&AS, 140, 261
Aoki, W., Ryan, S. G., Norris, J. E., et al. 2002, ApJ, 580, 1149
Aoki, W., Beers, T. C., Christlieb, N., et al. 2007, ApJ, 655, 492
Barbuy, B., Jorissen, A., Rossi, S. C. F., & Arnould, M. 1992, A&A, 262, 216
Barbuy, B., Spite, M., Spite, F., et al. 2005, A&A, 429, 1031
Beers, T. C., & Christlieb, N. 2005, ARA&A, 43, 531
Biémont, E., & Godefroid, M. 1980, A&A, 84, 361
Biémont, E., Grevesse, N., Hannaford, P., & Lowe, R. M. 1981, ApJ, 248, 867
Biémont, E., Palmeri, P., & Quinet, P. 1999, Ap&SS, 269, 635
Busso, M., Gallino, R., & Wasserburg, G. J. 1999, ARA&A, 37, 239
Busso, M., Gallino, R., Lambert, D. L., Travaglio, C., & Smith, V. V. 2001, ApJ, 557, 802
Carbon, D. F., Barbuy, B., Kraft, R. P., et al. 1987, PASP, 99, 335
Carretta, E., Gratton, R., Cohen, J. G., Beers, T. C., & Christlieb, N. 2002, AJ, 124, 481
Cayrel, R. 1988, Data Analysis, in The Impact of Very High S/N Spectroscopy on Stellar Physics (Dordrecht: Kluwer), ed. G. Cayrel de Strobel, & M. Spite, 345
Cayrel, R., Depagne, E., Spite, M., et al. 2004, A&A, 416, 1117
Clayton, D. D. 1988, MNRAS, 234, 1
Clegg, R. E. S., Tomkin, J., & Lambert, D. L. 1981, ApJ, 250, 262
Costes, M., Naulin, C., & Dorthe, G. 1990, A&A, 232, 270
del Peloso, E. F., Cunha, K., da Silva, L., & Porto de Mello, G. F. 2005, A&A, 441, 1149
Depagne, E., Hill, V., Spite, M., et al. 2002, A&A, 390, 187
Drake, N. A., & Pereira, C. B. 2007, CNO and Li abundances in Barium-enriched stars, in Convection in Astrophysics, ed. F. Kupka, I. Roxburgh, & K. Chan, 304
Drake, N. A., & Pereira, C. B. 2008, AJ, 135, 1070

Drake, J. J., & Smith, G. 1991, MNRAS, 250, 89
Edvardsson, B., Andersen, J., Gustafsson, B., et al. 1993, A&A, 275, 101
Engleman, R. Jr., & Rouse, P. E. 1975, J. Quant. Spectrosc. Rad. Transf., 15, 831
Fagotto, F., Bressan, A., Bertelli, G., & Chiosi, C. 1994, A&AS, 104, 365
Fehrenbach, C., & Duflot, M. 1981, A&A, 101, 226
François, P., Depagne, E., Hill, V., et al. 2003, A&A, 403, 1105
Goriely, S., & Mowlavi, N. 2000, A&A, 362, 599
Gratton, R. G. 1989, A&A, 208, 171
Gratton, R. G., & Sneden, C. 1988, A&A, 204, 193
Gratton, R. G., & Sneden, C. 1994, A&A, 287, 927
Grevesse, N., & Sauval, A. J. 1998, Space Sci. Rev., 85, 161
Grieve, G. R., & Madore, B. F. 1986, ApJS, 62, 427
Hartwick, F. D. A., & Cowley, A. P. 1985, AJ, 90, 2244
Hannaford, P., Lowe, R. M., Grevesse, N., Biémont, E., & Whaling, W. 1982, ApJ, 261, 736
Hill, V., Barbuy, B., Spite, M., et al. 2000, A&A, 353, 557
Hobbs, L. M., Thorburn, J. A., & Rebull, L. M. 1999, ApJ, 523, 797
Huang, Y., Barts, S. A., & Halpern, J. B. 1992, J. Phys. Chem., 96, 425
Johnson, D. R. H., & Soderblom, D. R. 1987, AJ, 93, 864
Jonsell, K., Edvardsson, B., Gustafsson, B., et al. 2005, A&A, 440, 321
Kaufer, A., Stahl, O. Tubbesing, S., et al. 1999, The Messenger, 95, 8
Korn, A. J., Shi, J., & Gehren, T. 2003, A&A, 407, 691
Kupka, F., Piskunov, N. E., Ryabchikova, T. A., Stempels, H. C., & Weiss, W. W. 1999, A&AS, 138, 119
Kurucz, R. L. 1993, CD-ROM 13, Atlas9 Stellar Atmosphere Programs and 2 km s^{-1} Grid, Cambridge, Smithsonian Astrophys. Obs
Lambert, D. L. 1981, The chemical composition of red giants – The first dredge-up phase, ed. I. Iben, & A. Renzini, in Physical Process in Red Giants (Dordrecht: D. Reidel Publ. Co.), 115
Lambert, D. L., Heath, J. E., Lemke, M., & Drake, J. 1996, ApJS, 103, 183
Lucatello, S., Gratton, R., Cohen, J. G., et al. 2003, AJ, 125, 875
Lucatello, S., Tsangarides, S., Beers, T. C., et al. 2005, ApJ, 625, 825
McWilliam, A., Preston, G. W., Sneden, C., & Searle, L. 1995, AJ, 109, 2757
Marsakov, V. A., & Borkova, T. V. 2006, Astron. Lett., 32, 545
Martin, G. A., Fuhr, J. R., & Wiese, W. L. 1988, J. Phys. Chem. Ref. Data, 17, 4
Mashonkina, L., Gehren, T., Shi, J.-R., Korn, A. J., & Grupp, F. 2011, A&A, 528, A87
Masseron, T., van Eck, S., Famaey, B., et al. 2006, A&A, 455, 1059
Masseron, T., Johnson, J. A., Blez, B., et al. 2010, A&A, 509, 28
Nissen, P. E., Primas, F., Asplund, M., & Lambert, D. L. 2002, A&A, 390, 235
Pereira, C. B., & Drake, N. A. 2009, A&A, 496, 791
Pompéia, L., Hill, V., Spite, M., et al. 2008, A&A, 480, 379
Pradhan, A. D., Partridge, H., & Bauschlicher, C. W. 1994, J. Chem. Phys., 101, 3857
Preston, G. W., & Sneden, C. 2001, ApJ, 122, 1545
Reddy, B. E., Tomkin, J., Lambert, D. L., & Allende Prieto, C. 2003, MNRAS, 340, 304
Reyniers, M., Van Winckel, H., Gallino, R., & Straniero, O. 2004, A&A, 417, 269
Ryan, S. G., Norris, J. E., & Beers, T. C. 1996, ApJ, 471, 254
Ryan, S. G., Aoki, W., Norris, J. E., & Beers, T. C. 2005, ApJ, 635, 349
Shetrone, M., Martell, S. L., Wilkerson, R., et al. 2010, AJ, 140, 1119
Sivarani, T., Bonifacio, P., Molaro, P., et al. 2004, A&A, 413, 1073
Smith, G., Edvardsson, B., & Frisk, U. 1986, A&A, 165, 126
Smith, V. V., Cunha, K., Jorissen, A., & Boffin, H. M. J. 1996, A&A, 315, 179
Smith, V. V., Lambert, D. L., & Nissen, P. E. 1998, ApJ, 506, 405
Sneden, C. 1973, Ph.D. Thesis, Univ. of Texas
Sneden, C. 1983, PASP, 95, 745
Sneden, C., Gratton, R. G., & Crocker, D. A. 1991, A&A, 246, 354
Sneden, C., McWilliam, A., Preston, G. W., et al. 1996, ApJ, 467, 819
Sobeck, J. S., Ivans, I. I., Simmerer, J. A., et al. 2006, AJ, 131, 2949
Thévenin, F., & Idiart, T. P. 1999, ApJ, 521, 753
Thompson, I. B., Ivans, I. I., Bisterzo, S., et al. 2008, ApJ, 677, 556
Tomkin, J., & Lambert, D. L. 1984, ApJ, 279, 220
Travaglio, C., Gallino, R., Arnone, E., et al. 2004, ApJ, 601, 864
van Winckel, H., & Reyniers, M. 2000, A&A, 354, 135
Van Eck, S., Goriely, S., Jorissen, A., & Plez, B. 2003, A&A, 404, 291
Vanture, A. 1992a, AJ, 103, 2035
Vanture, A. 1992b, AJ, 104, 1986
Vassiliadis, E., & Wood, P. R. 1993, ApJ, 413, 641
Venn, K. A., Irwin, M., Shetrone, M. D., et al. 2004, AJ, 128, 1177
Wiese, W. L., & Martin, G. A. 1980, NSDRS-NBS, 68
Wiese, W. L., Smith, M. W., & Miles, B. M. 1969, NBS Ref. Data. Ser.
Zacharias, N., Monet, D. G., Levine, S. E., et al. 2004, BAAS, 36, 1418

Pages 10 to 11 are available in the electronic edition of the journal at http://www.aanda.org

Table 1. Observed Fe I and Fe II lines. The $\log gf$ values were taken from Lambert et al. (1996).

Element	λ (Å)	χ(eV)	$\log gf$	EW_λ (mÅ)	$\log \varepsilon$
Fe I	5150.84	0.99	–3.000	138	5.72
	5198.71	2.22	–2.140	93	5.69
	5232.94	2.94	–0.080	143	5.55
	5242.49	3.63	–0.970	55	5.62
	5281.79	3.04	–0.830	101	5.58
	5288.52	3.69	–1.510	17	5.46
	5302.31	3.28	–0.740	97	5.73
	5307.36	1.61	–2.970	87	5.55
	5322.04	2.28	–2.840	42	5.54
	5339.93	3.27	–0.680	95	5.60
	5364.87	4.45	0.230	62	5.55
	5369.96	4.37	0.540	77	5.43
	5373.71	4.47	–0.710	21	5.72
	5389.48	4.42	–0.250	34	5.48
	5445.04	4.39	0.041	65	5.71
	5506.78	0.99	–2.800	144	5.48
	5554.90	4.55	–0.380	29	5.65
	5567.39	2.61	–2.560	38	5.57
	5569.62	3.42	–0.490	95	5.55
	5572.84	3.40	–0.280	106	5.52
	5576.09	3.43	–0.850	79	5.61
	5638.26	4.22	–0.720	24	5.47
	5686.53	4.55	–0.450	22	5.55
	5717.83	4.28	–0.979	20	5.70
	5762.99	4.21	–0.410	46	5.57
	6024.06	4.55	–0.060	52	5.72
	6027.05	4.08	–1.090	22	5.58
	6056.01	4.73	–0.400	20	5.65
	6065.48	2.61	–1.530	106	5.61
	6136.61	2.45	–1.400	133	5.74
	6137.69	2.59	–1.400	114	5.59
	6151.62	2.18	–3.290	30	5.54
	6173.34	2.22	–2.880	53	5.58
	6191.56	2.43	–1.420	118	5.45
	6200.32	2.60	–2.440	47	5.53
	6213.43	2.22	–2.480	73	5.48
	6230.72	2.56	–1.280	122	5.56
	6252.56	2.40	–1.720	109	5.55
	6265.13	2.18	–2.550	87	5.71
	6322.69	2.59	–2.430	51	5.56
	6393.60	2.43	–1.430	116	5.39
	6419.95	4.73	–0.090	32	5.59
	6421.35	2.28	–2.010	106	5.60
	6430.85	2.18	–2.010	120	5.68
	6592.91	2.72	–1.470	95	5.43
	6593.87	2.44	–2.420	78	5.73
	6750.15	2.42	–2.620	67	5.73
Fe II	5197.56	3.23	–2.250	75	5.60
	5234.62	3.22	–2.240	78	5.63
	5284.10	2.89	–3.010	48	5.41
	5325.56	3.22	–3.170	32	5.66
	5425.25	3.20	–3.210	30	5.63
	5534.83	3.25	–2.770	48	5.58
	6149.25	3.89	–2.720	18	5.62
	6247.55	3.89	–2.340	27	5.47
	6432.68	2.89	–3.580	32	5.58

Table 3. Other lines studied.

λ (Å)	Element	χ(eV)	$\log gf$	Ref.	EW_λ (mÅ)	$\log \varepsilon$
4571.10	Mg I	0.00	2.042e-06	A2007	134	5.89
4702.99	Mg I	4.34	3.020e-01	A2007	118	6.26
4102.94	Si I	1.91	7.943e-04	MCW	115	5.95
6155.14	Si I	5.62	1.698e-01	E93	23	6.07
6102.73	Ca I	1.88	1.621e-01	D2002	93	4.67
6122.23	Ca I	1.89	4.786e-01	D2002	124	4.73
6161.30	Ca I	2.52	5.370e-02	E93	22	4.75
6162.18	Ca I	1.90	8.128e-01	D2002	141	4.78
6166.44	Ca I	2.52	7.244e-02	R03	24	4.67
6169.04	Ca I	2.52	1.585e-01	R03	49	4.79
6169.56	Ca I	2.53	3.311e-01	DS91	56	4.60
6439.08	Ca I	2.52	2.951e+00	D2002	117	4.62
6455.60	Ca I	2.51	5.129e-02	R03	32	4.95
6471.66	Ca I	2.51	2.041e-01	S86	46	4.60
6493.79	Ca I	2.52	7.762e-01	DS91	92	4.76
5239.82	Sc II	1.45	1.698e-01	MFW	66	1.36
5526.82	Sc II	1.77	1.318e+00	MFW	79	1.06
5657.88	Sc II	1.51	2.884e-01	GS	64	1.10
5669.04	Sc II	1.50	7.586e-01	GS	66	1.70
6245.62	Sc II	1.51	9.555e-01	R03	67	1.56
6604.60	Sc II	1.36	5.012e-02	R03	34	1.09
4533.25	Ti I	0.85	3.388e+00	D2002	104	2.89
4534.78	Ti I	0.84	1.905e+00	D2002	95	2.96
4981.72	Ti I	0.84	3.162e+00	D2002	118	2.95
5866.46	Ti I	1.07	1.345e-01	E93	31	3.16
6126.22	Ti I	1.05	4.266e-02	R03	17	3.28
6261.10	Ti I	1.43	3.311e-01	B86	28	3.16
5296.70	Cr I	0.98	4.074e-02	GS	76	3.56
5300.75	Cr I	0.98	7.413e-03	GS	39	3.73
5345.81	Cr I	1.00	1.047e-01	GS	95	3.47
5409.80	Cr I	1.03	1.905e-01	GS	109	3.46
6330.09	Cr I	0.94	1.202e093	R03	18	3.91
5084.11	Ni I	3.680	6.607e-01	E93	42	4.42
5115.40	Ni I	3.834	5.248e-01	R03	27	4.40
6327.60	Ni I	1.68	7.709e-04	MFW	22	4.28
6767.77	Ni I	1.83	6.761e-03	MFW	67	4.24
7788.93	Ni I	1.95	1.023e-02	E93	55	3.96
4722.16	Zn I	4.01	4.074e-01	BG80	50	2.91
4810.53	Zn I	4.06	6.761e-01	BG80	47	2.67
4883.68	Y II	1.08	1.175e+00	SN96	86	0.41
5087.43	Y II	1.08	6.761e-01	SN96	64	0.14
5200.41	Y II	0.99	2.692e-01	SN96	52	0.20
5205.72	Y II	1.03	4.571e-01	SN96	62	0.19
6496.90	Ba II	0.60	4.170e-01	WM80	195	1.15
6320.42	La II	0.17	3.030e-02	VWR	32	–0.12
6390.48	La II	0.32	2.750e-02	S96	42	0.14
6774.33	La II	0.12	1.778e-02	S96	33	–0.02
4073.47	Ce II	0.48	2.089e+00	SN96	82	0.69
4120.84	Ce II	0.32	5.754e-01	SN96	69	0.67
4486.91	Ce II	0.30	4.365e-01	SN96	67	0.57
4562.37	Ce II	0.48	2.138e+00	SN96	84	0.47
4628.16	Ce II	0.52	1.820e+00	SN96	84	0.56
5274.24	Ce II	1.28	2.450e+00	VWR	42	0.43
6051.80	Ce II	0.23	2.512e-02	S96	16	0.40
4811.34	Nd II	0.06	9.660e-02	VWR	66	0.55
4959.12	Nd II	0.06	1.213e-01	VWR	73	0.56
4989.95	Nd II	0.63	2.377e-01	VWR	49	0.55

Table 3. continued.

λ (Å)	Element	χ(eV)	log gf	Ref.	EW_λ (mÅ)	log ε
5063.72	Nd II	0.98	1.746e-01	VWR	27	0.69
5089.83	Nd II	0.20	7.244E-02	E93	36	0.25
5130.59	Nd II	1.30	1.259e+00	SN96	50	0.69
5234.19	Nd II	0.55	3.467E-01	SN96	62	0.47
5249.58	Nd II	0.98	1.202e+00	SN96	60	0.45
5293.16	Nd II	0.82	6.310e-01	SN96	66	0.62
5311.46	Nd II	0.99	2.754e-01	SN96	27	0.47
5361.47	Nd II	0.68	3.981e-01	SN96	50	0.35
5431.54	Nd II	1.12	3.491e-01	VWR	19	0.33
5442.26	Nd II	0.68	1.259e-01	SN96	28	0.43
5740.88	Nd II	1.16	2.754e-01	VWR	23	0.56

References. A2007: Aoki et al. (2007); BG80: Biémont & Godefroid (1980); B81: Biémont et al. (1981); D2002: Depagne et al. (2002); DS91: Drake & Smith (1991); E93: Edvardsson et al. (1993); GS: Gratton & Sneden (1988); H82: Hannaford et al. (1982); MFW: Martin et al. (1988); MCW: McWilliam et al. (1995); PS: Preston & Sneden (2001); R03: Reddy et al. (2003); R04: Reyniers et al. (2004); S86: Smith et al. (1986); S96: Smith et al. (1996); SN96: Sneden et al. (1996); VWR: van Winckel & Reyniers (2000); WSM: Wiese et al. (1969); WM80: Wiese & Martin (1980).